Journal of
Synchrotron Radiation

ISSN 0909-0495

Received 15 September 2008
Accepted 26 January 2009

Characterization of germanium linear kinoform lenses at Diamond Light Source

L. Alianelli,[a]* K. J. S. Sawhney,[a] M. K. Tiwari,[a] I. P. Dolbnya,[a] R. Stevens,[b] D. W. K. Jenkins,[b] I. M. Loader,[b] M. C. Wilson[b] and A. Malik[b]

[a]Diamond Light Source Ltd, Didcot OX11 0DE, UK, and [b]STFC Micro-Nano Technology Centre, Didcot OX11 0QX, UK. E-mail: lucia.alianelli@diamond.ac.uk

The unprecedented brilliance achieved by third-generation synchrotron sources and the availability of improved optics have opened up new opportunities for the study of materials at the micrometre and nanometre scale. Focusing the synchrotron radiation to smaller and smaller beams is having a huge impact on a wide research area at synchrotrons. The key to the exploitation of the improved sources is the development of novel optics that deliver narrow beams without loss of brilliance and coherence. Several types of synchrotron focusing optics are successfully fabricated using advanced miniaturization techniques. Kinoform refractive lenses are being developed for hard X-ray beamlines, and the first test results at Diamond are discussed in this paper.

Keywords: synchrotron optics; micro-focusing; kinoform refractive lenses.

1. Introduction

The new synchrotron radiation facility of the UK, the Diamond Light Source, started user operations in January 2007. Since then 13 beamlines have become operational. By the end of 2012, academic and industrial users will have access to a total of 22 instruments. High-quality bent and bimorph mirrors are used at Diamond to focus the X-ray radiation. We have also started a programme to procure, design, fabricate and test in-line refractive (Snigirev *et al.*, 1996) and refractive–diffractive optics (Evans-Lutterodt *et al.*, 2003), made by micro-fabrication techniques such as e-beam lithography and deep reactive ion etching. Our aim is to deliver micro-focusing lenses for Diamond users on a day-to-day basis, and to improve design, fabrication and testing methods to achieve nano-focusing. Multi-level quasi-kinoform zone plates for the focusing of hard X-rays were first discussed and fabricated by Di Fabrizio *et al.* (1999). An efficiency of 50% at very high X-ray energies, up to $E = 50$ keV, was demonstrated by Kamijo *et al.* (2006).

Kinoform lenses are based on refraction, like compound refractive lenses (CRLs). However, unlike in CRLs, efficiency and effective aperture are not limited by absorption but rather by technological challenges. The use of a phase profile in a kinoform lens allows minimization of the path length of the radiation in the lens material. Therefore kinoform planar lenses are considered ideal devices for nano-focusing applications. Our first tests of silicon kinoform micro-focusing lenses showed transmission over 50% of the monochromatic beam and effective aperture, measured with a scan of the direct beam width, of 200 μm at $E = 12$ keV (Alianelli *et al.*, 2007). In April 2008 we started to collect data from micro-focusing lenses for the first time at the new bending-magnet Test beamline B16. In this paper we illustrate the experimental set-up at B16 and discuss the measured focusing efficiency.

2. Design and fabrication of kinoform lenses

The properties of CRLs and kinoform lenses have already been discussed thoroughly (Evans-Lutterodt *et al.*, 2003; Alianelli *et al.*, 2007; Schroer *et al.*, 2005; Aristov *et al.*, 2000; Nöhammer *et al.*, 2003; Jark *et al.*, 2006). More recently, arrays of kinoform lenses leading to a focused hard X-ray beam with convergence exceeding the critical angle were presented (Evans-Lutterodt *et al.*, 2007). For arrays of nano-focusing lenses, it is best to use refractive surfaces with decreasing radii (Schroer & Lengeler, 2005).

Geometric aberrations are minimized in these arrays using parabolic or elliptical refractive surfaces. The ideal shape for an X-ray refractive surface depends on the degree of collimation of the incident radiation and on the size and distance of the source. To a certain extent the ideal shape of the refractive surfaces is chosen by ray-tracing simulations. Diffraction effects are not simulated however.

The focal length of an array of X-ray lenses of the same shape can be approximated by $f = R/N\delta$, where R is the radius of curvature at the apex of the surface, N is the number of refractive surfaces and δ is the refractive index real part decrement,

$$\delta = \mathrm{Re}(1 - n) \simeq 10^{-5}\text{–}10^{-6}. \quad (1)$$

Modern micro-fabrication methods permit lenses to be made with radii smaller than 1 μm; therefore a lens made of a single refractive surface and $f \leq 1$ m can be fabricated.

Table 1
Parameters of some of the lenses fabricated in Si and Ge.

Data are only shown for $f = 1000$ mm and phase shift between steps of 2π. These lenses are based on a single-element elliptical refractive surface. The radius at the apex decreases with increasing energy: Ge lenses have larger radii than Si ones, and hence are preferred for very hard X-rays.

	X-ray energy (keV)	Radius at apex (μm)	Geometrical aperture (μm)	Length of steps (μm)
Silicon	8	7.7	1350	20
	10	4.9	1050	25
	12	3.4	900	30.5
	14	2.5	750	36
	16	1.9	650	41
	18	1.5	550	46
	20	1.2	500	51
Germanium	20	2.5	760	25
	40	0.61	380	51
	60	0.27	250	76
	80	0.15	190	102
	100	0.097	150	127

Several geometrical parameters of the lenses fabricated for Diamond are listed in Table 1. The kinoform profile illustrated in Fig. 1 allows absorption minimization of the X-ray beam. The step length L depends on the X-ray wavelength and refractive index: $L = \lambda/\delta$. The step width W decreases with increasing aperture, starting from a few micrometres at the lens centre.

By approximating the shape of a kinoform segment by a triangle, the mean path length of radiation in each segment is $\langle l \rangle \simeq L/2$. Therefore the ideal kinoform lens transmission is

$$T = \exp(-\mu\langle l \rangle) \simeq \exp(-\mu\lambda/2\delta). \quad (2)$$

For easier fabrication, some lateral additional thickness t is added to the lens profile, as shown in Figs. 1 and 2. This increases absorption and reduces the effective aperture. The extra thickness does not change the kinoform phase profile as

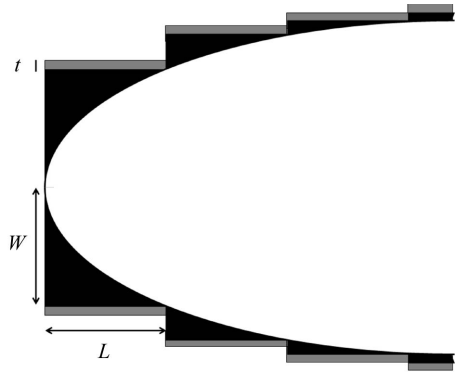

Figure 1
Drawing of a section of an elliptical kinoform lens. The step length L is equal to the ratio of the wavelength to the refractive index decrement. In a kinoform lens with a phase shift of 2π or 4π, L varies between 20 and 130 μm, depending on the energy and material (see Table 1). The step width W decreases with increasing aperture, starting from a few micrometres at the lens centre. The additional thickness t added to the lens, for easier fabrication, is shown in grey. The lenses described in this paper have $t = 4$ μm.

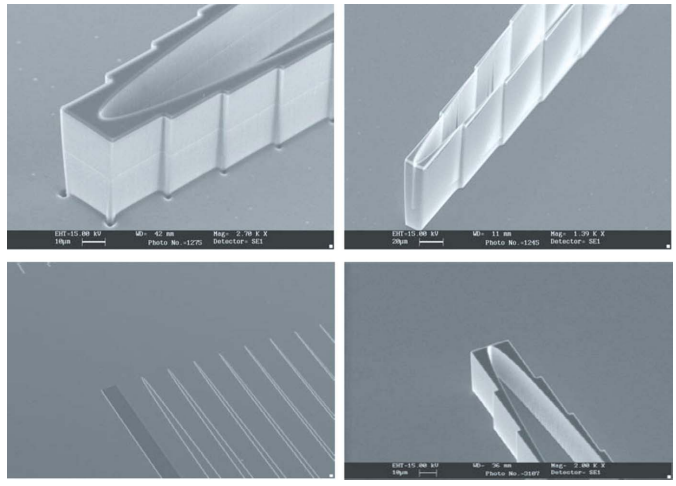

Figure 2
Scanning electron micrographs of silicon (top) and germanium (bottom) kinoform lenses fabricated at Diamond and STFC. The silicon lenses are designed for $E = 8$ to 20 keV, the germanium lenses for $E = 20$ to 150 keV.

it simply changes the phase of the radiation passing through it by

$$\Delta\varphi = \varphi_{\rm air} - \varphi_{\rm material} = 2\pi\frac{1-n}{\lambda}L = 2\pi. \quad (3)$$

Focusing takes place at the elliptical surface, therefore the extra thickness only affects the amount of transmitted intensity. This can be quantified in the following way: the outermost kinoform segments are extremely thin, hence the mean path length of radiation becomes $\langle l \rangle \simeq L$. The central part of the lens contributes with transmission T as calculated in equation (2), while the external part, where the segments are very thin, contributes with

$$T_{\rm ext} = \exp(-\mu\langle l \rangle) \simeq \exp(-\mu\lambda/\delta). \quad (4)$$

Using equations (2) and (4), it is easy to see that the theoretical efficiency of a kinoform lens exceeds 90% above 10 keV for silicon and above 40 keV for germanium. As shown in Table 1, for $E = 20$ keV, the radius of a single element kinoform lens is $R = 1.2$ and 2.5 μm for silicon and germanium, respectively. Therefore we choose germanium lenses for $E >$ 20 keV, as fabrication is easier. Moreover, the etch depth of Ge is higher than that of Si, for a given thickness of the hard mask material, for instance 100 nm of an aluminium nitride mask.

The gain of a focusing device is the ratio of the flux density in the focal spot to the flux density in the same area, without lens. It can be calculated also as

$$G = T \times A/\sigma, \quad (5)$$

where A is the aperture and σ is the focused beam size. Gain of about 1000 can be achieved, in a one-dimensional focusing geometry, provided that the effective aperture is of the order of 1000 μm and the focused spot $\sim$1 μm.

Pre-patterned silicon and germanium lenses were etched by using a modified Bosch process. The maximum depth achieved so far is just above 100 μm. SU8 was used as a mask for the Si

lenses shown at the top of Fig. 2. A deposition process to deliver aluminium nitride and silicon oxide hard masks with very high selectivity and purity is being developed. The aim is to produce lenses with thicknesses up to 500 μm in silicon and germanium. Scalloping is a well known problem associated with the Bosch process, and has to be minimized for the fabrication of nano-focusing synchrotron optics. Modern plasma etch tools exist that deliver etched walls with less than 20 nm peak-to-valley scalloping features.

3. Experimental

Measurements were performed at the Test beamline B16, which is set up on a bending magnet of Diamond Light Source. The full width at half-maximum (FWHM) photon source size is 126 μm × 56 μm (horizontal × vertical). The beamline comprises a water-cooled fixed-exit double-crystal monochromator that provides monochromatic beams over a 2–20 keV energy range. Downstream of the monochromator is a toroidal mirror that normally focuses the X-ray beam with 1:1 magnification at 44 m downstream of the source. For measurements reported here, however, the mirror was retracted from the beam path to allow unfocused monochromatic beam to be incident on the lenses. The kinoform lenses and the detector systems were installed on a versatile optics table, which is located at the downstream end of the beamline's experimental hutch. The optics table has three multi-axis motorized stations for installing the optics, the diagnostics and the detector. Tests of the focusing optics with focal lengths from 200 mm up to more than 1000 mm are possible. For measurements involving shorter focal length optics or for planar lenses in crossed geometry, miniature stages from Attocube in Germany are used. Beam demagnification and gain from Ge elliptical lenses at E = 20 keV were measured at B16 using gold wire scans and a high-resolution imaging detector. An area detector with an effective pixel size of 6.5 μm was employed to align the lenses. Fluorescence scans of a 50 μm-thick Au wire were used to precisely measure the size of the focused beam and the intensity gain. The fluorescence was recorded with a detector at 45° in front of the Au wire. The experiment is located at 47 m from a bending-magnet source.

Crossed lenses are used to produce focusing in both the vertical and horizontal planes. Two perpendicular Ge lens wafers are mounted on Attocube piezo-stages, properly translated and rotated, in order to obtain a point focus. The vertical and horizontal focusing lenses have $f_{\rm vertical}$ = 1080 mm and $f_{\rm horizontal}$ = 1000 mm, respectively, and are mounted at a distance of 80 mm. The set-up is shown in Fig. 3. Elliptical lenses etched on the germanium wafers can be seen. Only the lenses for E = 20 keV were used; lenses for different energy are easily inserted by translating the wafers.

A low-resolution image of two perpendicular lenses arrays in a 20 keV monochromatic beam is shown in Fig. 4. The shadow of the lenses and the partially focused spots from several lenses can be clearly seen. These spots come from lenses designed for different energy values (30 keV, 40 keV *etc.*). A detector with improved resolution was used to image the focused spot in Fig. 5. The detector is based on a PCO4000 CCD camera, equipped with a 20× objective and a 7 μm-thick Ce:YAG scintillator. The effective pixel size in Fig. 5 is 0.18 μm. We do not have a measurement of the detector resolution in this configuration. However, this can be calculated as it depends on the scintillator thickness, objective numerical aperture and wavelength of the light collected by the CCD camera (Koch *et al.*, 1998). The calculated resolution is approximately 2 μm. The measured spot size is less than 3 μm, both in the vertical and horizontal planes, whilst the expected spot is elliptical, like the X-ray source. The round spot observed is either caused by limited detector resolution

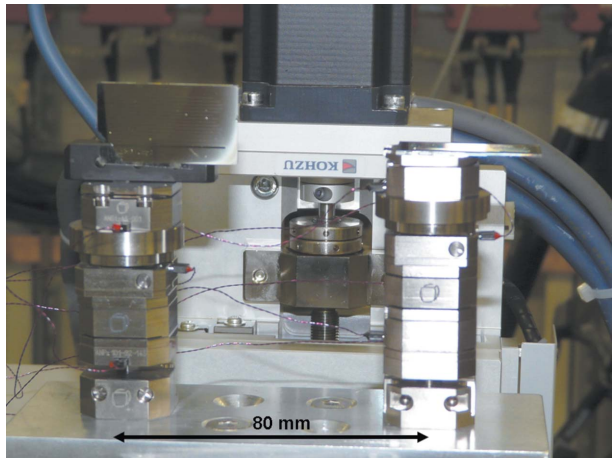

Figure 3
Arrangement used to align two crossed lenses, separated by 80 mm. The Ge wafers with the etched lenses are visible. To be able to obtain a stigmatic image, the two lenses were fabricated with 80 mm difference in their focal lengths. Each wafer is mounted on top of several piezo-stages for the alignment. The entire system is carried by one of the stages on the optics test bench at B16 of Diamond.

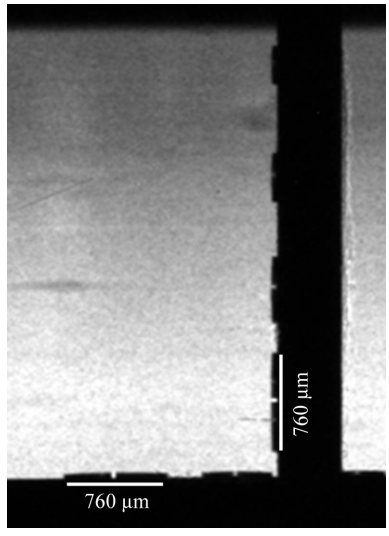

Figure 4
Low-resolution image of the crossed wafers in a monochromatic beam at E = 20 keV, refracted by the arrays of lenses. The shadows of the wafers and several lenses are clearly visible. Several focused spots are visible as well, including those from lenses designed for $E \neq 20$ keV.

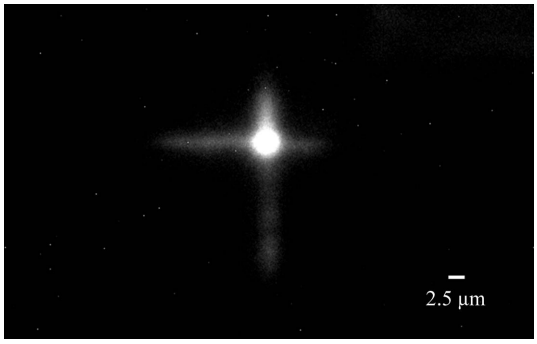

Figure 5
High-resolution image of a beam delivered by two crossed germanium lenses in the set-up shown in Fig. 3. The beam size is less than 3 μm.

or by the mismatch between the lens height (50 μm) and the lens aperture (760 μm geometrical *versus* 200 μm effective). In order to maximize the gain when using crossed planar lenses, matching apertures and heights have to be used. Therefore it is mandatory to make deeper lenses.

The beam size from the vertically focusing lens was measured with better accuracy using the wire scan. The raw data, and the derivative, are shown in Fig. 6: the beam size FWHM is 1.3 μm, in good agreement with the demagnification ratio of 47:1 and vertical source size of 56 μm. We show the data fitting with a Gaussian profile. The best fit would actually be a Lorentzian function; therefore our measurements are likely to suffer from unwanted scattering, probably from the lens surface. The plots in Fig. 6 represent the raw data, without any wire size deconvolution; additional uncertainty in the focused beam shape and size might originate from wire thickness, non-uniformity and non-perfect alignment.

The intensity gain of the linear focus (*i.e.* vertically focusing lens only) was measured using the ratio of the fluorescence signal from the focused beam to that of the direct unfocused beam, normalized with the ratio of wire thickness to focus FWHM. This is an approximate method, which gives $G \simeq 32$, at least one order of magnitude less than expected. The measurement of the gain *via* the fluorescence scan is not very precise.

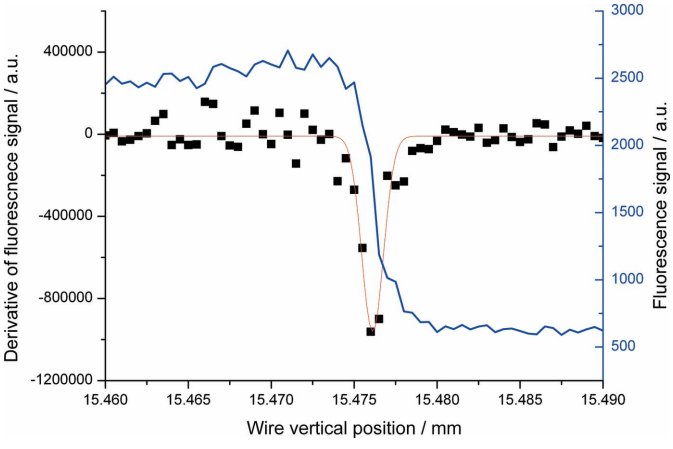

Figure 6
Fluorescence signal from a gold wire scan (blue line) in the focal plane of a germanium lens, with $f = 1080$ mm and $E = 20$ keV. The derivative of the raw data and fit result, with a Gaussian function with a FWHM of 1.3 μm (red line), are also shown.

Alternatively, the gain can be estimated using equation (5), with the lens effective aperture and transmission data measured in previous experiments (Alianelli *et al.*, 2007, 2009). The effective aperture is equal to the width of the lens that contributes with focused X-ray intensity. The effective aperture is smaller than the geometrical aperture because of the absorption discussed in §2. A scan of the incident beam size was used to determine the effective aperture, obtaining $A \simeq 200$ μm for these lenses. Using the measured transmission $T = 50\%$ we therefore obtain $G \simeq 77$. A better effective aperture is normally measured using smaller or more coherent beams. There is much scope for improvement of lens quality as well, and therefore we believe that the gain of new kinoform nano-focusing lenses will reach 1000, for focusing in one plane only.

4. Summary and conclusions

The level of miniaturization achieved by modern micro-fabrication technology has permitted the realisation of several types of advanced synchrotron optics, such as lenses, zone plates, waveguides, capillaries and hybrid systems such as multilayer Laue lenses. In-line compact focusing optics, based on refraction, are being designed and fabricated for use in hard and very hard X-ray beamlines at Diamond.

We have presented experimental results from novel germanium lenses at $E = 20$ keV with a focused beam of 1.3 μm. These are promising optics for very hard X-rays, and more tests are planned for energy up to 80 keV at a wiggler beamline. A proper measurement of flux gain is necessary, since it is not clear whether the low gain measured is caused by the low-resolution measurements or by the quality and thickness of the lens walls.

The good fabrication control achieved for these lenses is witnessed by the large aperture, which contains hundreds of kinoform steps. However, wall roughness and scalloping are problems that are being seriously tackled as we have a plan to deliver Si and Ge nano-focusing lenses.

Hard mask technologies that will allow deeper etch whilst keeping the walls of the lens as thin as possible are being developed as well. This will deliver better acceptance in the plane perpendicular to focusing, from the current 100 μm to 500 μm.

The high brightness of the X-ray sources at Diamond will soon allow nano-focusing tests to be conducted. Our data show that the kinoform lenses fabricated so far have an excellent effective aperture; therefore they are suitable for nano-focusing applications, like planar compound refractive lenses. We fabricated lenses with $f = 200$ mm and are improving our experimental method (resolution and stability) to measure the smaller focused beams that these short focal lenses can deliver.

The fabrication of focusing lenses was funded by STFC Center for Instrumentation and by the STFC grant ST/

F001665/1. We acknowledge Diamond Light Source Ltd for providing beam time on B16. Technical support for the experiment set-up was given by A. Malandain and H. Patel.

References

Alianelli, L., Sawhney, K. J. S., Jenkins, D. W. K., Loader, I. M., Stevens, R., Snigirev, A. & Snigireva, I. (2007). *Proc. SPIE*, **6705**, 670507.

Alianelli, L., Sawhney, K. J. S., Tiwari, M. K., Dolbnya, I. P., Stevens, R., Jenkins, D. W. K., Loader, I. M., Wilson, M. C. & Malik, A. (2009). *Proceedings of the International Conference on X-ray Microscopy, Journal of Physics Conference Series.* In the press.

Aristov, V., Grigoriev, M., Kuznetov, S., Shabelnikov, L., Yunkin, V., Weitkamp, T., Rau, C., Snigireva, I., Snigirev, A., Hoffmann, H. & Voges, E. (2000). *Appl. Phys. Lett.* **77**, 4058–4060.

Di Fabrizio, E., Romanato, F., Gentili, M., Cabrini, S., Kaulich, B., Susini, J. & Barrett, R. (1999). *Nature (London)*, **401**, 895–898.

Evans-Lutterodt, K., Ablett, J., Stein, A., Kao, C., Tennant, D., Klemens, F., Taylor, A., Jacobsen, C., Gammel, P., Huggins, H., Bogart, G., Ustin, S. & Ocola, L. (2003). *Opt. Expr.* **11**, 919–926.

Evans-Lutterodt, K., Stein, A., Ablett, J. M., Bozovic, N., Taylor, A. & Tennant, D. M. (2007). *Phys. Rev. Lett.* **99**, 134801.

Jark, W., Pérennès, F. & Matteucci, M. (2006). *J. Synchrotron Rad.* **13**, 239–252.

Kamijo, N., Suzuki, Y., Tamura, S., Takeuchi, A. & Yasumoto, M. (2006). *Proceedings of the 8th International Conference on X-ray Microscopy, IPAP Conference Series 7*, pp. 97–99.

Koch, A., Raven, C., Spanne, P. & Snigirev, A. (1998). *J. Opt. Soc. Am. A*, **15**, 1940–1951.

Nöhammer, B., Hoszowska, J., Freund, A. K. & David, C. (2003). *J. Synchrotron Rad.* **10**, 168–171.

Schroer, C. G., Kurapova, O., Patommel, J., Boye, P., Feldkamp, J., Lengeler, B., Burghammer, M., Riekel, C., Vincze, L., Van der Hart, A. & Kuchler, M. (2005). *Appl. Phys. Lett.* **87**, 124103.

Schroer, C. G. & Lengeler, B. (2005). *Phys. Rev. Lett.* **94**, 054802.

Snigirev, A., Kohn, V., Snigireva, I. & Lengeler, B. (1996). *Nature (London)*, **384**, 49–51.